Indian Journal of Science and Technology, Vol 9(38), DOI: 10.17485/ijst/2016/v9i38/90171, October 2016
ISSN (Print) : 0974-6846
ISSN (Online) : 0974-5645

CFD Analysis of Thermal Performance in Isosceles Right Triangle Rib Roughness on the Absorber Plate Solar Air Heater

Rajeev Ranjan*, M. K. Paswan and N. Prasad

Mechanical Engineering Department, National Institute of Technology Jamshedpur, Jamshedpur-831014, Jharkhand,India; rajeev3278@yahoo.co.in, mkpaswan.me@nitjsr.ac.in, India; nprasad.me@nitjsr.ac.in

Abstract

Objective: This paper provides analytical investigation of flow and roughness parameters on average heat transfer and flow friction characteristics of an artificial roughness solar air heater having isosceles right triangle ribs on the absorber plate. **Methods/Statistical Analysis:** Artificial roughness having isosceles right triangle geometry is developed for breaking laminar sub-layer. In CFD simulation different parameter like Reynolds no-3593 to 15000, duct aspect ratio=5:1, relative roughness pitch (P/e) i.e. 3.33-40(12 values) and relative roughness height (e/D) i.e. 0.015-0.045(3 values) taken. **Findings:** In all cases the average Nusselt number tends to increase as Reynolds number increases. The average friction factor has been found to be 3.45 times over the smooth duct. It has been observed that the average friction factor tends to decrease as the Reynolds number increases. Increment in Thermal performance obtained for Maximum thermo-hydraulic performance is obtained for relative roughness pitch of 5 and relative roughness height 0.045. **Applications/ Improvements:** The applications of solar air heaters are space heating and drying. Recent time solar air heater is very important in rolling agriculture purpose, heating and cooling of the room and industrial applications.

Keywords: CFD, Heat Transfer, Isosceles Right Triangle Rib, Thermo-hydraulic Performance Parameter

1. Introduction

Solar air heater is a simple device for heating air by employing solar energy. Various designs of solar air heater with different shapes have been recommended to enhance thermal performance of solar air heaters by using artificial roughness. Several designs for the enhancement of heat transfer coefficient and hence the improvement of thermal performance of solar air heaters have been proposed and investigated by a number of investigators.[1] investigated the purpose of artificial roughness in the form of small diameter wire on the top absorber plate to enhance thermal performance in a solar air heater.[2] investigated the effect of transverse wire roughness.[3] worked on expanded metal mess roughness.[4] studied on rectangular ducts with repeated chamfered rib-roughness.[5] carried out experiment on transverse wire rib roughness.[6] investigated the effect of 90° broken ribs.[7] worked on rib-grooved roughness. Nusselt number and friction factor correlations were also developed by authors.[8] investigated the effect of grit geometry. [9]worked on dimple-shaped artificial roughness. It is found that maximum Nusselt number correspond to relative roughness (e/D) of 0.0379 and relative pitch (P/e) of 10.[10] investigated integral repeated discrete square ribs on the absorber plate.[11] worked on the effect of multiple v- rib roughness on artificial roughened solar air heater. The maximum heat transfer enhancement was found to occur for a relative roughness width (W/w) value of 6 while friction factor attains maximum value for relative roughness width (W/w) value of 10.[12] investigated a rectangular duct roughened with w-shaped rib.[13] investigated thermal performance of wire-screen metal mesh as artificially roughened on the underside of the absorber plate. Authors investigated that decreasing wire pitch, thermal performance of solar air heater increases.[14] investigated thermo-hydraulic performance evaluation using

*Author for correspondence

w-discrete rib in solar air heater.Authors find maximum Nusselt number along the friction factor is 2.79 and 1.98 as compare to smooth plate. [15]have conducted an experimental approach towards the study of transverse wedge artificial roughness. [16]studied on heat transfer enhancement in packed bed solar air heater.Authors find that packed bed solar air heater having with lower porosity performs better than higher porosity. [17]investigated evaluation of thermal performance of wire mesh solar air heater.Authors concluded that by adding 5 % low carbon steel wire mesh increase in overall efficiency.[18–20] have carried out CFD analysis of various geometries including triangular, circular transverse wire ribs, square sectioned transverse ribs, and equilateral triangle sectioned ribs. Authors have simulated the above geometries using ANSYS Design MODULAR V 12.1 and RNG k-ε turbulence model reported good agreement with[21] and [22]empirical correlations.[23] used FLUENT 6.1 CFD Code and SST k-ε as a turbulence model for analysis of ten different types of ribs, namely rectangular, square, chamfered, triangular and so forth. FLUENT 6.3.26 Code and renormalization group (RNG) k-ε turbulence model was used by[24] to simulate artificial roughness. [25]have carried out simulation of fluid flow and heat transfer in a solar air heater duct with metal grit as a roughness element of circular, square and triangular cross section, having an angle of attack 54°, 56°, 58°, 60°and 62°, were tested on small Reynolds number. [26]worked on v-shaped ribs roughness underside of the absorber plate by using CFD. The result shows good agreement with the experimental results.The objectives of the present CFD analysis is to investigate the effect of relative roughness (P/e) and relative roughness height (e/D) on Nusselt number and Friction factor, and also find the best rib configuration in terms of thermo-hydraulic performance parameter.

2. CFD Simulation

CFD simulation of two-dimensional artificially roughened solar air heater duct along transverse ribs roughness with isosceles right triangle cross-section as a vortex generator in inlet section is carried out using the CFD software package ANSYS FLUENT (version 14.5). The general assumption, consider in the analysis are as follows:

1. The flow is two dimensional, steady and turbulent.
2. The walls in contact with fluid are assigned, no-slip boundary condition.
3. The flow is single phase across the duct.
4. The thermodynamic properties of air and the absorber plate (aluminum) are considered constant.
5. The effect of radiation heat transfer and other heat losses are considered less.

The widespread availability of computational power at reasonable rate with its span of application from modeling to simulation, designing optimization and manufacturing had shifted the preference towards this approach of the study. Earlier only structural and thermal analysis was done on computers, but with an advance in the field of CFD, now even fluid flow systems are simulated. The accuracy of these solutions can be justified only by comparison with experimental results. So computational approach can be seen as a bridge between theoretical and experimental approach, to be more precise it can be considered as a hub for designing and research.

2.1 Computational Solution Domain

The model designed and simulated for the study of artificial roughness in solar air heater is in accordance with the ASHRAE Standard 93-2003[27]. According to these standards whole flow field is divided into three sections i.e. the entry section, the test section and the exit section. The first section is the entry section and is provided so that the flow is fully developed before entering into the test section. The artificial roughness to be investigated is used in the test section. The exit section is provided to make sure that the effect of flow exit is not affecting the test section. The geometric model developed for the current study is as shown in Figure 1.

The modeling software used here is ANSYS Design Modeler v 14.5. Due to the nature of the study domain, a 2D problem is modeled in the study. The model was created as a surface geometry. The geometry consists of three sections, namely entry section, test section and exit section which are 225mm, 125mm and 115mm long respectively. The duct height is 20mm and an absorber plate of 0.5mm thickness is placed above the test section. The entry section is provided so that the flow becomes fully developed before it enters the test section. The exit section is provided to avoid the end effect from travelling upstream into the test section (as the flow is sub-sonic). According to ASHRAE standards 93-2003, an entrance and exit length of $5\sqrt{WH}$ and $2.5\sqrt{WH}$ respectively are provided[27]. The created geometry for smooth and rough plate is shown in Figure 2 (a) & Figure 2 (b).

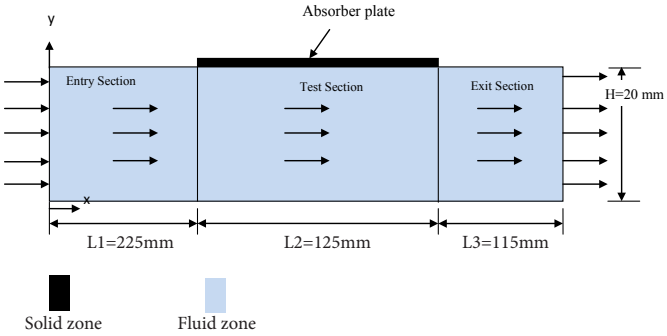

Figure 1. Computational domain.

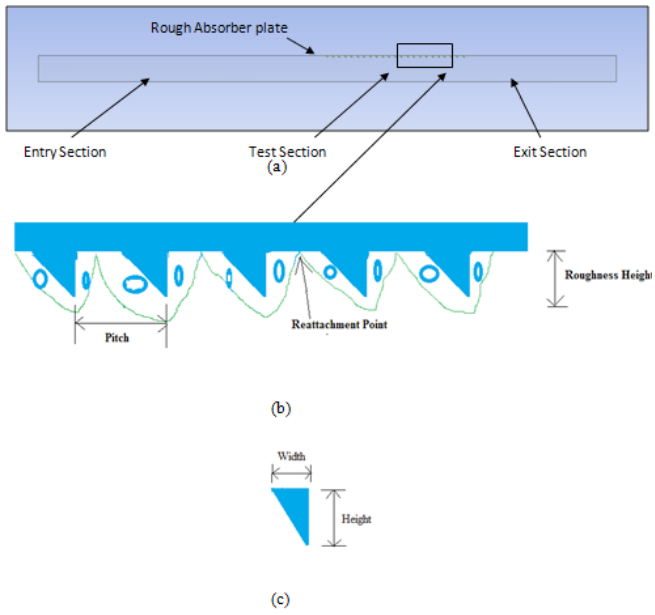

Figure 2. (a) Roughened plate(b) Magnified view (c) Rib shape.

2.2 Boundary Conditions

The study domain consists of a rectangular duct in x-y plane, which is extruded along the z - direction. The inlet is given as velocity-inlet boundary condition. The outlet is given as pressure-an outlet boundary condition with pressure being equal to atmospheric condition. The top-surface of the study domain is given as a constant heat flux boundary condition with heat flux being equal to solar insolation. The working fluid in all cases is taken as air and absorber plate material is taken as aluminum. The thermo-physical properties of the material used are shown in Table 1. No-slip boundary condition is given along the wall.

The turbulence intensity at the core of fully developed flow is calculated using the empirical correlation given:

$$I = 0.16\, Re^{-\frac{1}{8}} \quad (1)$$

The material properties are shown in Table 2.

The range of operating parameters employed in this computational investigation is shown in Table 3.

2.3 Geometry Meshing

The meshing software used here is [29]ICEM CFD V 14.5. To obtain better results the entire fluid flow zone is sub-divided into many zones and a combination of structured (mapped) and unstructured mesh was created in the fluid domain. The fluid flow zone near the roughness element was further refined to reduce the cell size to 0.025mm in order to determine laminar sub-layer. The meshed geometry with quad element, generated for 5mm pitch

Table 1. Boundary condition of study domain

Surface	Boundary Condition	Value
Inlet (Test Section)	*Velocity-inlet ($u=U_0$, $v=0$, $T=T_0$)*	Calculated from Re
Outlet (Test Section)	*Pressure-outlet ($\partial u/\partial x=0$, $\partial v/\partial x=0$, $\partial t/\partial x=0$)*	0 Pascal (gauge)
Top surface	*Wall (Starting $u=0$, $v=0$, $\partial T/\partial y=0$)*	Heat flux=1000W/m^2
Bottom surface	*Wall (Starting $u=0$, $v=0$, $\partial T/\partial y=0$)*	Adiabatic wall

Table 2. Properties of the materials used in the computational domain

Properties	Air	Aluminum
Density, 'ρ' (kg/m^3)	1.225	2719
Specific Heat, 'C_p'(J/kg-K)	1006.43	871
Thermal Conductivity 'k' (W/m-K)	0.0242	202.4
Viscosity, 'μ' (N/m^2)	1.7894x10^{-5}	-

Table 3. Range of operating parameters for CFD analysis

Operating Parameters	Range
Uniform flux, 'q'	1000W/m^2
Reynolds number, Re	3593-15000(6 values)
Relative Roughness pitch, 'P/e'	3.33-40(12 values)
Relative Roughness height,(e/D)	0.015-0.045(3 values)
Prandtl number, 'Pr'	0.7441

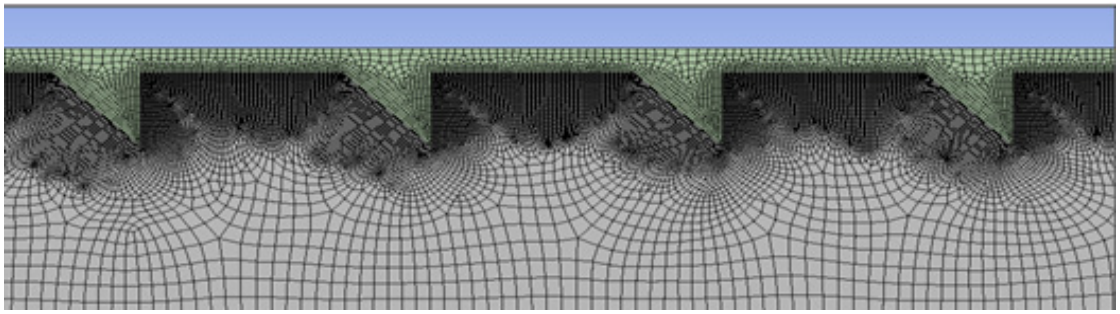

Figure 3. Mesh geometry.

and 0.5mm roughness height geometry having 221730 numbers of cells is as shown in Figure 3. A grid independence test has been done over grids with different number of cells. It can be observed that the variation in Nusselt number and friction factor slightly increases when moving from 211,226 cells to 236,886. Increasing number of cells beyond this value does not give required advantages. Thus, the grid system of 211,226 cells is adopted for the current computation.

2.4 Governing Equations and Data Reduction

The flow field in this problem is governed by steady state, two dimensional, incompressible hence continuity, conservation of momentum, and energy equations are used to solve the forced turbulent fluid flow and heat transfer in the artificially roughened solar air duct. The governing equations in the rectangular Cartesian coordinate system can be written as follows:-

Continuity equation:

$$\frac{\partial}{\partial x_i}(\rho u_i) = 0 \tag{2}$$

Momentum equation:

$$\frac{\partial}{\partial x_i}(\rho u_i u_j) = -\frac{\partial P}{\partial x_i} + \frac{\partial}{\partial x_j}\left[\mu\left(\frac{\partial u_i}{\partial x_j} + \frac{\partial u_j}{\partial x_i}\right)\right] + \frac{\partial}{\partial x_j}\left(-\rho\overline{u_i' u_j'}\right) \tag{3}$$

Energy equation:

$$\frac{\partial}{\partial x_i}(\rho u_j T) = \frac{\partial}{\partial x_j}\left((\Gamma + \Gamma_t)\frac{\partial T}{\partial x_j}\right) \tag{4}$$

where, Γ and Γ_t are molecular thermal diffusivity and turbulent thermal diffusivity respectively.

$$\Gamma = \frac{\mu}{\mathrm{Pr}} \text{ and } \Gamma_t = \frac{\mu_t}{Pr_t}$$

Eq. (2) to (4) is called Reynolds Averaged Navier-Stokes equation (RANS). The additional term $-\rho\overline{u_i' u_j'}$ in eq. (3) is called Reynolds stress and is responsible for capturing the effects of turbulence. But this additional term requires us to add two more equations in order to get a closed form of equation. A common way is to use Boussinesq Hypothesis to relate the Reynolds stress to mean velocity gradient as given below

$$-\rho\overline{u_i' u_j'} = \mu_t\left(\frac{\partial u_i}{\partial x_j} + \frac{\partial u_j}{\partial x_i}\right) \tag{5}$$

The Boussinesq hypothesis is implemented here using RNG k-epsilon turbulence model.

Equation for Renormalization-group (RNG) k-epsilon turbulence model:

$$\frac{\partial}{\partial x_i}(\rho k u_i) = \frac{\partial}{\partial x_j}\left(\alpha_k \mu_{eff}\frac{\partial k}{\partial x_j}\right) + G_k - \rho\varepsilon \tag{6}$$

$$\frac{\partial}{\partial x_i}(\rho \varepsilon u_i) = \frac{\partial}{\partial x_j}\left[\alpha_\varepsilon \mu_{eff}\frac{\partial \varepsilon}{\partial x_j}\right] + C_{1\varepsilon}G_k\frac{\varepsilon}{k} - C_{2\varepsilon}\rho\frac{\varepsilon^2}{k} - R_\varepsilon \tag{7}$$

where, μ_{eff} is the effective turbulent viscosity and μ_t is the turbulent viscosity and is given by

$$\mu_{eff} = \mu + \mu_t \tag{8}$$

$$\mu_t = \rho C_\mu \frac{k^2}{\varepsilon} \tag{9}$$

In eq. (6) and (7), G_k represents the creation of turbulence kinetic energy due to the mean velocity gradients and is specified by

$$G_k = -\frac{\rho\overline{u_i' u_j'}\left(\partial u_j\right)}{\partial x_i} \tag{10}$$

$C_{1\varepsilon}$, $C_{2\varepsilon}$, C_μ, α_k and α_ε are constants and their respective default values are: $C_{1\varepsilon}$=1.42, $C_{2\varepsilon}$=1.68, C_μ=0.0845, α_k=1.39 and α_ε=1.39[30].

Use of the transverse ribs with isosceles right triangle results enhancement in heat transfer, which is predicted by calculating average Number for the roughened solar

air heater. This enhancement is also accompanied by an increase in friction factor. The friction is calculated from pressure drop, Δ P across the cross- section of artificial roughened solar air heater.

The average Nusselt number for artificially roughened solar air heater is computed as

$$Nu = \frac{h.D}{k} \tag{11}$$

where,*h* is the average heat transfer coefficient.

The average friction factor for artificially roughened solar air heater

$$f = \frac{\Delta p.D}{2\rho l v^2} \tag{12}$$

The performance of solar air heater using artificial roughness results enhancement of air heater and enhancement of friction losses. It is sensible to design the artificial roughness in such a way that it breaks the laminar sublayer at the wall without disturbing the existing turbulent flow in order to keep the pressure low. Thus, it is increases the heat transfer coefficient between absorber plate & the flowing air. Finally the heat transfer increases with the minimum heat losses. Also the addition of artificial roughness increases additional friction factor that leads to additional pumping power.

For the optimum performance, we should consider both the thermal effect, i.e. the enhancement in heat transfer rate and also the hydraulic effect i.e. the increase in pressure drop across the duct. To consider both these effects together the thermo-hydraulic performance is calculated. An alternate form of this equation using Stanton number was first proposed by[28]. It is defined as

$$\eta_{THPP} = \frac{Nu_r/Nu_s}{\left(f_r/f_s\right)^{\frac{1}{3}}} \tag{13}$$

where, Nu is the Nusselt number and f is the friction factor. The subscript r and s signify rough and smooth absorber plate.

The friction factor and the Nusselt number for the smooth absorber plate where taken from the semi-empirical relations. The friction factor was calculated from[22].

$$f_s = 0.0791\ Re^{-0.25} \tag{14}$$

The Nusselt number for the smooth absorber plate was calculated from[21].

$$Nu_s = 0.023\ Re^{0.8} Pr^{0.4} \tag{15}$$

3. Validation of the Model

The friction factor and Nusselt number determined from CFD data for smooth duct have been compared with the values obtained from[22] and [21]respectively. The average percentage deviation of the CFD data of friction factor and Nusselt number from the values predicted by correlation has been found to ±8.5% and ±9%. Figures 4 and 5 shows the comparison of CFD data and predicted values of friction factor and Nusselt number respectively. This shows good agreement between CFD data obtained from present work and a predicted value establishes the accuracy of the value taken from CFD analysis.

4. Results and Discussion

In this section effects of fluid flow characteristics of roughened absorber on heat transfer and friction factor

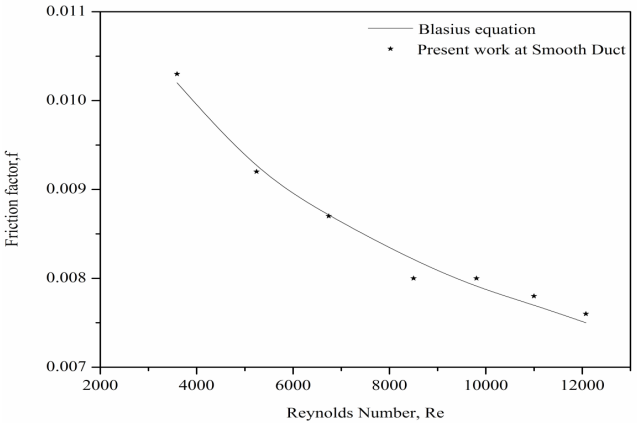

Figure 4. Comparison of friction factor present work and Blasius equation for smooth duct.

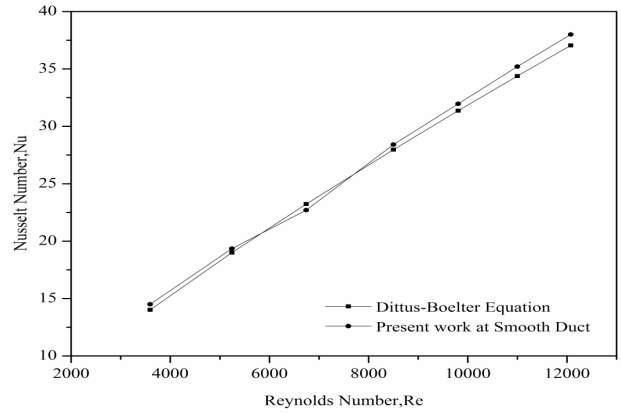

Figure 5. Comparison of Nusselt number present work and Dittus-Boelter equation for smooth duct.

are presented. Results are also compared with smooth absorber plate under similar condition.

4.1 Grid Independence Test

The grid independence test was conducted on artificially roughened solar air heater provided a transverse rib roughness with isosceles right triangle cross-section. Six sets of grids with different number of cells 45878, 50885, 64706, 116722, 211226 and 236886 are tested for the geometry of e=1.5mm and P=15mm at a Reynolds number of 15000. The parameter used to relate the sensitivity of the grid was friction factor and Nusselt number. The results of the grid sensitivity test are shown in Table 4. It can be seen that the relative error falls within an acceptable range as the number of elements is increased to 236886. The improvement in results over the last set of grid is not significant, so the number of elements is chosen as 211226. Thus, the grid system of 211226 cells is adopted for the current computation.

4.2 Effect of Reynolds Number

Figures 6 and 7 show us the contour plots for velocity magnitude at different Reynolds number. It is observed that average Nusselt number increases with increase in Reynolds number. This is due to turbulence created by the ribs increases turbulence kinetic energy and turbulence dissipation rate, which in turn breaks the laminar sub layer thickness and increases the heat transfer coefficient. It further reduces thermal resistance in the direction of flow result in increasing in Nusslet number. This reduction in the boundary thickness increases the heat transfer rate. Figures 8 and 9 show us the contour plots for static temperature at different Reynolds number. It can be seen that as the Reynolds number increases the static temperature of the flow field decreases. It can also be observed that the diffusion of temperature into the core of the flow field decreases as the Reynolds number increases, but the near wall diffusion of temperature increases as the Reynolds number increases. Figures 10 and 11 show us the contour plots for turbulence intensity at different Reynolds number. It can be seen that the peak value of the turbulent intensity is found on the top of rib front region and it decreases with an increase in the distance from the wall. This can be attributed to the formation of eddies in the vicinity of the wall due to the high shear stress which defuses in the main flow. Presence of isosceles right triangle sectional rib causes an additional loss of energy resulting in increase in average friction factor than smooth. It can also see that average friction factor decreases with the increase in Reynolds number because of the suppression in laminar sub layer. Figure 12 shows friction factor versus Reynolds Number for different values of P/e i.e.3.3 to 13.33 and fixed value of e/D=0.045. Figure 13 shows Nusselt number versus Reynolds Number for different values of P/e and fixed value of e/D=0.045. It has been found that Nusselt number tends to increases with an increase in Reynolds number. This is due to the presence of isosceles right triangle rib roughness on the absorber plate lead to better heat transfer performance on the secondary flow induced by the top rib. Secondary flow has two counter-rotating vortices, carry cold fluid from the central core region toward the rib wall. This secondary flow interacts with main flow which affects the flow reattachment and recirculation between transverse ribs.

Table 4. Grid Independence Test

No. of cells	Nu (CFD)	f (CFD)	% difference Nu	% difference f
45878	47.16220755	0.033068542	-------	-----
50885	51.2123328	0.033026622	7.90849592	0.1269279
64706	54.90088677	0.032390052	6.71856902	1.9653256
116722	56.58735034	0.031218411	2.98028368	3.7530449
211226	54.67315748	0.030424434	2.37459393	2.2530476
236886	54.65854386	0.030394283	0.03325473	0.0943948

4.3 Effect of Relative Roughness Pitch

Figure 14 shows friction factor versus Relative roughness pitch for different values of Reynolds number and fixed value of e/D=0.045. From the plots we can interpret that in general the relative roughness pitch increases with decrease in friction factor for a given value of relative roughness height. Figure also shows that with increase

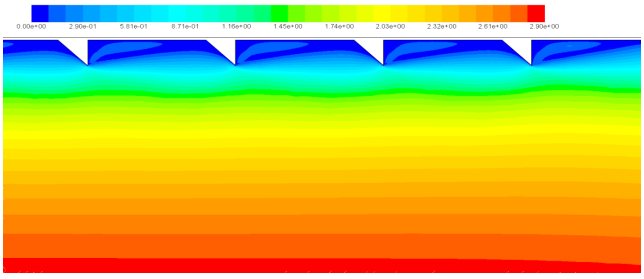

Figure 6. Contour plot for velocity magnitude for e=1.0 P=5 Re=5000.

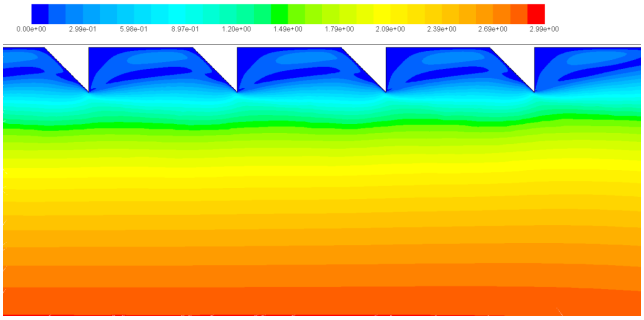

Figure 7. Contour plot for velocity magnitude for e=1.5 P=5 Re=5000.

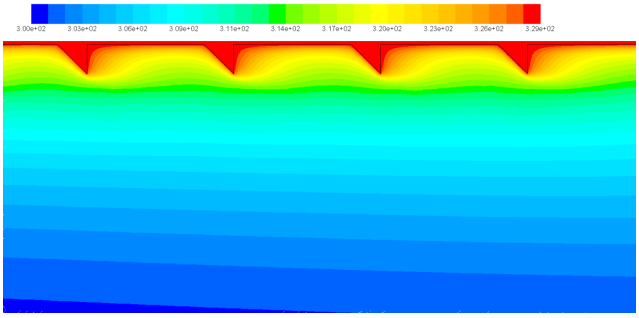

Figure 8. Contour plot for static temperature for e=1.0 P=5 Re=5000.

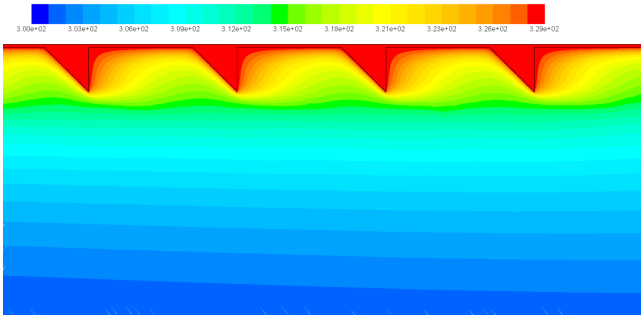

Figure 9. Contour plot for static temperature for e=1.5 P=5 Re=5000.

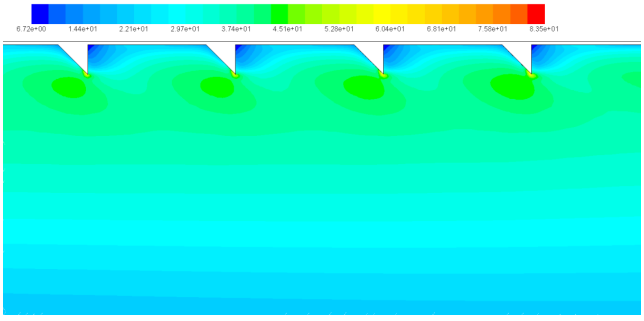

Figure10. Contour plot for turbulence intensity for e=1.0 P=5 Re=5000.

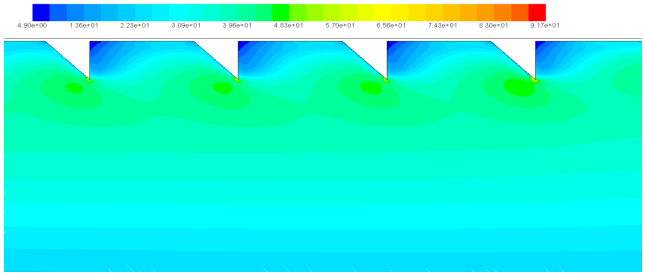

Figure 11. Contour plot for turbulence intensity for e=1.5 P=5 Re=5000.

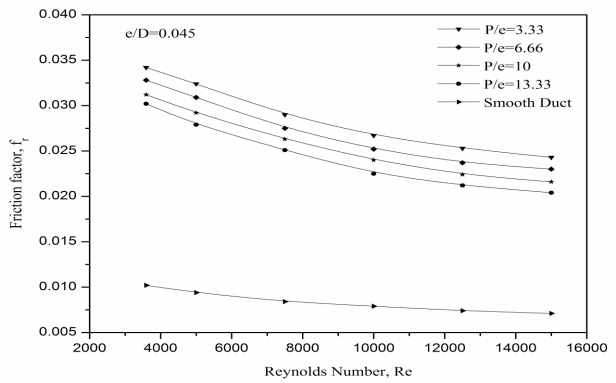

Figure 12. Friction factor versus Reynolds Number for different values of P/e and fixed value of e/D=0.045.

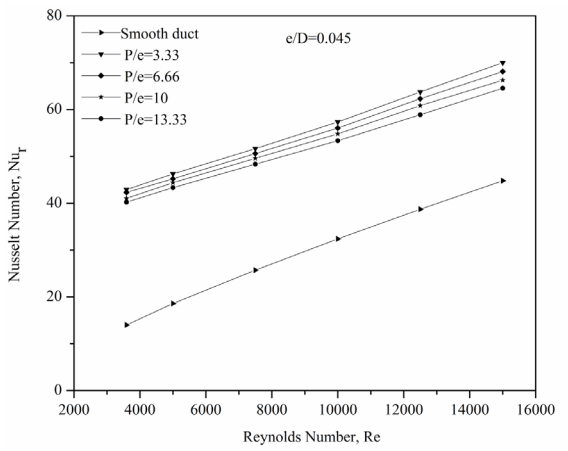

Figure 13. Nusselt number versus Reynolds Number for different values of P/e and fixed value of e/D=0.045.

in friction factor, value of Reynolds numberdecreases. A possible explanation for this peak is that the roughness element is protruding outside the laminar sub-layer there by interrupting the primary flow region. The roughened duct with relative roughness pitch 3.33 provides maximum friction factor for all ranges of parameter. Figure 15 shows Nusselt number versus Relative roughness pitch

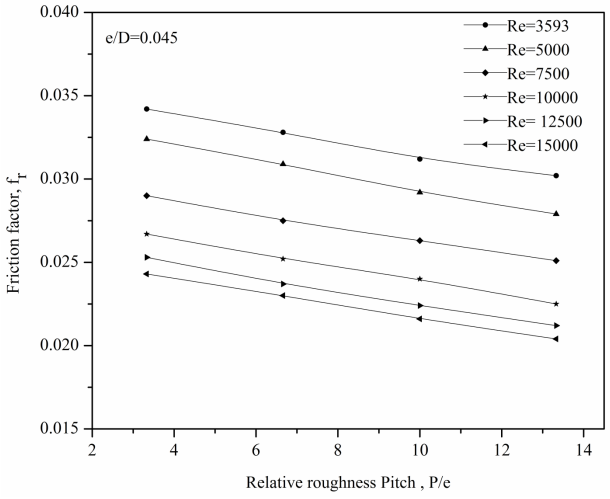

Figure14. Friction factor versus Relative roughness pitch for different values of Reynolds number and fixed value of e/D=0.045.

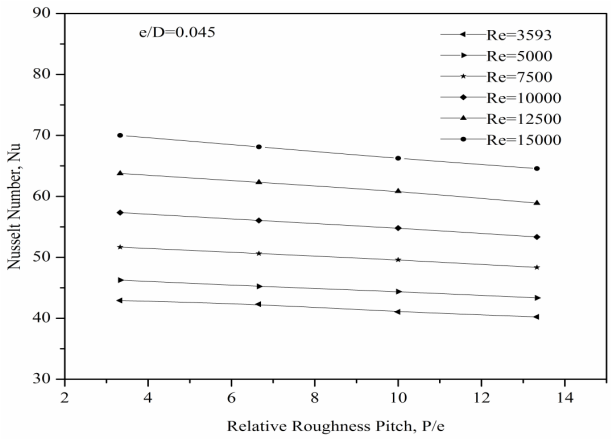

Figure 15. Nusselt number versus Relative roughness pitch for different values of Reynolds number and fixed value of e/D=0.045.

for different values of Reynolds number and fixed value of e/D=0.045. It is seen that increasing the value of relative roughness Pitch, it decreases the value of Nusselt number. Figure also shows that Nusselt number decrease with an increase of Reynolds number. Isosceles right triangle rib with relative roughness Pitch 3.33 gives the high Nusselt number for all ranges of Reynolds number. Isosceles right triangle rib with relative roughness Pitch of providing the high Nusselt number for all ranges of Reynolds number. This is due to increase in the number of reattachment points of air with the inside surface of the absorber plate. The flow has a higher pitch 20 mm reattaches whereas for low pitch 5mm it may not have reattachment at all.

4.4 Effect of Roughness Height

Figure 16 shows that friction factor versus Relative roughness height e/D for different values of Reynolds number and fixed value of P/e=10. It is observed that friction factor increases with an increase in relative roughness height. For a given value of e/D results more interruption in the flow path. From the plots we can see that as the roughness height increases the friction factor increases for all values of pitch. Figure 17 Friction factor versus Reynolds number for different values of e/D and fixed value of P/e=10. Isosceles right triangle rib with relative roughness height of (e/D= 0.045) gives the highest friction factor.

Figure 18 Nusselt number versus Relative roughness height e/D for different values of Reynolds number and fixed value of P/e=10.It is found that Nusselt number increases with the change in value of e/D. Isosceles right triangle rib with e/D=0.045 gives the highest Nusselt number. Figure 19 shows Nusselt number versus Reynolds number for different values of e/D and fixed value of P/e=10. It is seen that the value of Nusselt number increases with an increase in relative roughness height at fixed value of P/e=10.

5. Thermo-hydraulic Performance

Figure 20 shows Thermo-hydraulic performance versus Reynolds number of all values of roughness height and roughness pitch. It is found that THPP values lies between 1.68 to 3.02.It is found that isosceles right triangle sectioned transverse rib roughness on the absorber

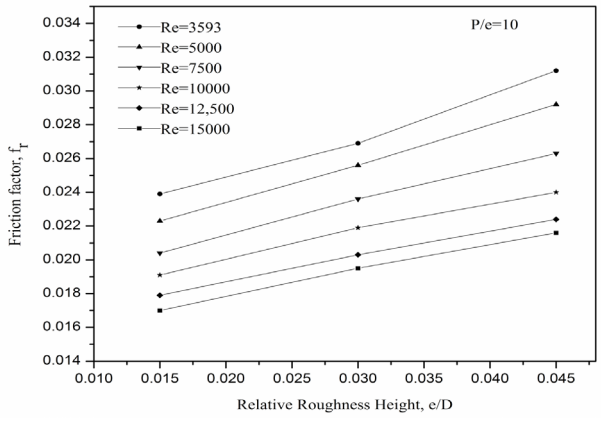

Figure 16. Friction factor versus Relative roughness height e/D for different values of Reynolds number and fixed value of P/e=10.

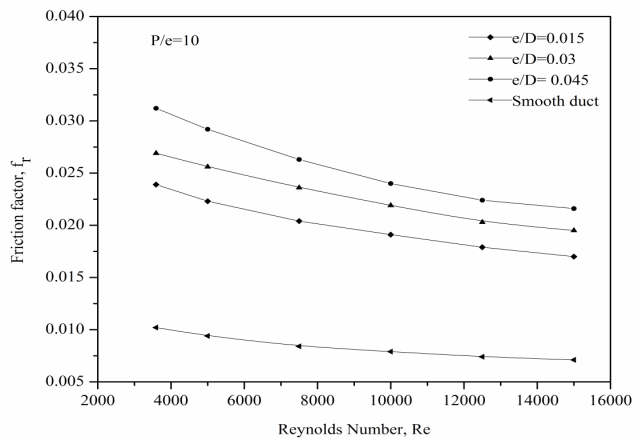

Figure 17. Friction factor versus Reynolds number for different values of e/D and fixed value of P/e=10.

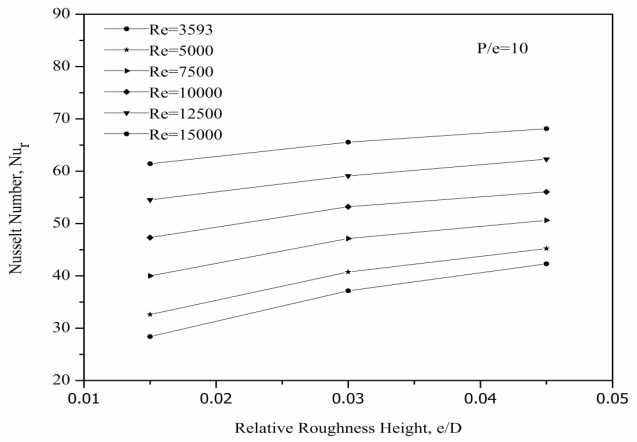

Figure 18. Nusselt number versus Relative roughness height e/D for different values of Reynolds number and fixesd value of P/e=10.

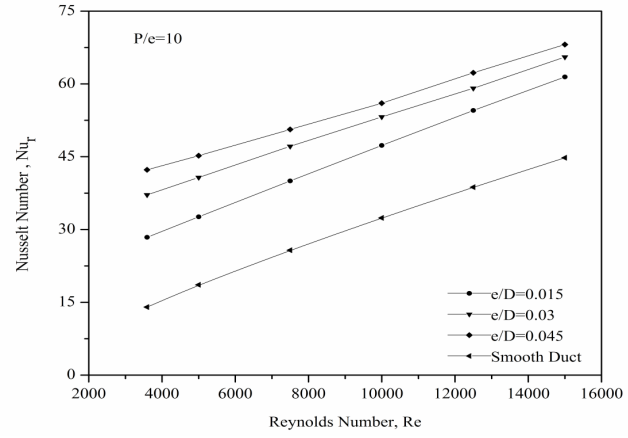

Figure 19. Nusselt number versus Reynolds number for different values of e/D and fixed value of P/e=10.

plate with Pitch(P)=5mm and rib (e)=1.5mm gives better thermal performance.

To validate the present numerical model, the results are compared with experimental results of [32](1988) and [31](2013) Expt. Work. Figure 21 showsNusselt number predicted by present work compared with[32] and[31]. The variation between experimental results of[32] (1988) and [31](2013) with present work is less than ±10%.The comparison of friction factor present CFD work and [32] shown in Figure 22. The variation between experimental results of [32] and present work is less than ±12% The results are also compared with available experimental results with different roughness geometries of similar trends for heat transfer and fluid friction for[1,2,5,15,33,31,34] under similar flow condition shown. These trends show good agreement with experimental and CFD work.It has been observed that the model i.e. isosceles right triangle rib having artificial roughened solar air heater predicts the experimental data quite accurate.

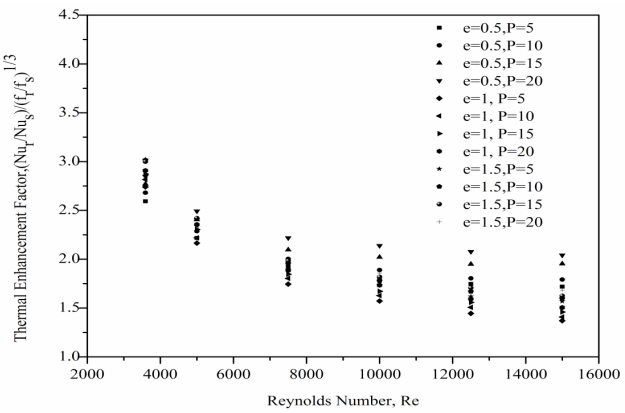

Figure 20. Thermo-hydraulic performance versus Reynolds number of all values of roughness height and roughness pitch.

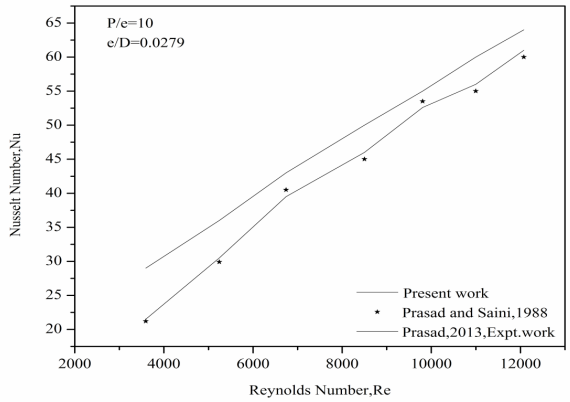

Figure 21. Nusselt number predicted by present work compared with Prasad and Saini and Prasad.

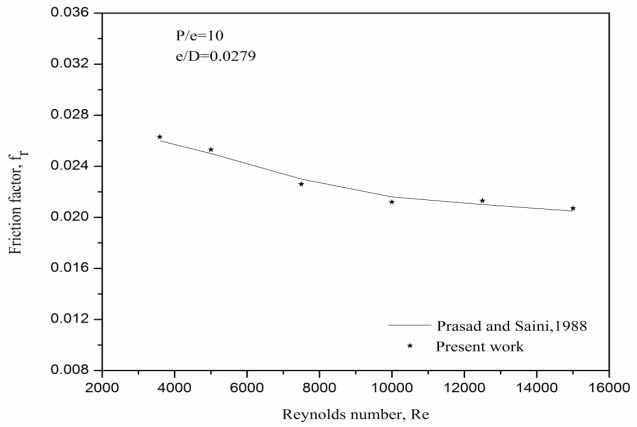

Figure 22. Friction factor predicted by present work compared withPrasad and Saini.

6. Conclusions

A CFD analysis to fluid flow and heat transfer characteristics of solar air heaters having roughened duct provided with artificial roughness in isosceles right triangle shape. Nusselt number has been found increase with increase in Reynolds number where friction factor decreases with increase in Reynolds number. The maximum Nusselt number and Friction factor found at relative roughness height 0.045.The CFD simulation is validated with Dittus-Boelter empirical relationship for smooth duct. Maximum thermo-hydraulic performance is obtained for relative roughness pitch of 5 and relative roughness height 0.045.

7. Nomenclature

L1 Entrance length, mm
L2 Test section length, mm
L3 Exit length, mm
e Roughness height, mm
l Projected length of metal grit perpendicular to direction of flow, mm
s Projected length of metal grit parallel to direction of flow, mm
K Thermal conductivity of air, W/mk
f Friction factor
P Roughness pitch length, mm
D Hydraulic diameter, mm
C_p Specific heat of air, J/kg K
W Width of duct, mm
H Height of duct, mm
T Temperature, K
K Turbulence kinetic energy
I Turbulence intensity
Nu Nusselt number
Re Reynolds number
Pr Prandtl Number
St Stanton Number

Subscripts

S Smooth
R Roughened
T Turbulent
A Ambient
I Inlet
O outlet
F Fluid

Greek symbols

Φ Chamfer angle, deg
α Angle of attack, deg
θ Groove angle, deg
ΔP Pressure drop, pa
E Rate of dissipation
η_{THP} Thermo-Hydraulic Performance

Acronyms

SIMPLE Semi-Implicit method for pressure linked equations
THPP Thermo-Hydraulic Performance Parameter

8. References

1. Prasad K, Mullick SC. Heat transfer characteristics of a solar air heater used for drying purposes. Applied Energy. 1983; 13(2):83–93.
2. Gupta D, Solanki SC, Saini JS. Heat and fluid flow in rectangular solar air heater ducts having transverse rib roughness on absorber plates.Solar Energy. 1993; 51(1):31–7.
3. Saini RP, Saini JS. Heat transfer and friction factor correlations for artificially roughened ducts with expanded metal mesh as roughened element.International Journal of Heat and Mass Transfer. 1997; 40:973–86.
4. Karwa R, Solanki SC,Saini JS.Heat transfer coefficient and friction factor correlations for the transitional flow regime in rib-roughened rectangular ducts.International Journal of Heat Mass transfer. 1999; 26,1597–615.
5. Verma SK, Prasad BN. Investigation for the optimal thermohydraulic performance of artificially roughened solar air heaters.Renewable Energy.2000; 20:19–36.
6. Sahu MM, Bhagoria JL. Augumentation of heat transfer coefficient by using 90° broken transverse ribs on absorber plate of solar air heater, Renewable energy. 2005; 30:2057–63.

7. Layek A, Saini JS, Solanki SC. Heat transfer and friction characteristics of artificially roughened ducts with compound turbulators.International Journal of Heat and Mass Transfer. 2007; 50, 4845–54.
8. Karmare SV, Tikekar AN. Heat transfer and friction factor correlation for artificially roughened ducts with metal grit ribs,International Journal of Heat and Mass Transfer.2009; 50:4342–51.
9. Saini RP, Verma J. Heat transfer and friction factor correlations for a duct having dimple- shaped artificial roughness for solar air heaters.Energy. 2008; 33:1277–87.
10. Aharwal KR,Gandhi BK, Saini JS.Heat transfer and friction characteristics of solar air heater ducts having integral inclined discrete ribs grits on absorber plate.International Journal of Heat and Mass Transfer. 2009; 52:2834–48.
11. Hans VS, Saini RP, Sain JS. Heat transfer and friction factor correlations for a solar air heater duct roughened artificially with multiple v-ribs.Solar Energy.2010; 84:898–911.
12. Lanjewar A, Bhagoria JL, Sarviya RM.Heat transfer and friction in solar air heater duct with W-shaped rib roughness on absorber plate.Energy. 2011; 36:6651–60.
13. Paswan MK, Sharma SP.Thermal performance of wire-mesh roughened solar air heaters.Arabian Journal for Science and Engineering. 2009; 1:31–40.
14. Rohit AK, lanjewar A. Thermo-hydraulic performance evaluation using w-discrete rib in solar air heater. Indian Journal of Science and Technology. 2016 May; 9(17). DOI:10.17485/ijst/2016/v9i17/89056.
15. Bhagoria JL, Saini JS, Solanki SC. Heat transfer coefficient and friction factor correlations for rectangular solar air heater duct having transverse wedge shaped rib roughness on the absorber plate.Renewable Energy. 2002; 25:341–69.
16. Lalji MK, Sarviya RM, Bhagoria JL. Heat transfer enhancement in packed bed solar air heater. Indian Journal of Science and Technology. 2011 Jul; 4(7).DOI:10.17485/ijst/2011/v4i7/30104.
17. Velmurugan P, Ramesh P. Evaluation of thermal performance of wire mesh solar air heater. Indian Journal of Science and Technology. 2011 Jan; 4(1).DOI:10.17485/ijst/2011/v4i1/29923.
18. Yadav AS, Bhagoria JL. A CFD based heat transfer and fluid flow analysis of a solar air heater provided with circular transverse wire rib roughness on the absorber plate.Energy. 2013; 55:1127–42.
19. Yadav AS, Bhagoria JL. Numerical investigation of flow through an artificially roughened solar air heater. International Journal of Ambient Energy. 2013.
20. Yadav AS, Bhagoria JL. A CFD based thermo –hydraulic performance analysis of an artificially roughened solar air heater having equilateral triangular sectioned rib roughness on the absorber plate. International Journal of Heat and Mass Transfer. 2013; 70:1016–39.
21. McAdams WH.Heat transmission. New York, McGraw-Hill; 1942.
22. Fox W, Pritchard P, Mc Donald A.Introduction to fluid mechanics. New York, John Wiley and Sons; 2010. p. 754.
23. Chaube A, Sahoo PK, Solanki SC. Analysis of heat transfer augmentation and flow characteristics due to rib roughness over absorber plate of a solar air heater.Renewable Energy. 2006; 31:317–31.
24. Kumar S, Saini RP. CFD based performance analysis of a solar air heater duct provided with artificial roughness, Renewable Energy. 2009; 34:1285–91.
25. Karmare SV, Tikekar AN. Analysis of fluid flow and heat transfer in a rib grit roughened surface solar air heater using CFD.Solar Energy.2010; 84:409–17.
26. Sharma AK, Thakur NS. CFD based fluid flow and heat transfer analysis of a v-shaped roughened surface solar air heater. International Journal of Engineering Science and Technology.2012; 4(5):2115–21.
27. ASHRAE Standard 93-2003. Method of testing to determine the thermal performance of solar collector; 2003.
28. Webb RL, Eckert ERG. Application of rough surface to heat exchanger design. International Journal of Heat and Mass Transfer. 1972; 15:1647–58.
29. ANSYS FLUENT. SAS analytical products 14.5. Documentation. ANSYS, Inc : USA ; 2003–4.
30. Launder BE, Splading DB. Lectures in mathematical models of turbulence. Academic Press, London: UK; 1972.
31. Prasad BN. Thermal performance of artificially roughened solar air heaters.Solar Energy. 2013; 91:59–67.
32. Prasad BN, Saini JS. Effect of artificial roughness on heat transfer and friction factor in a solar air heater.Solar Energy. 1988; 41(6):555–60.
33. Varun A, Patnaik, Saini RP, Singal SK, Siddartha. Performance prediction of solar air heater having roughened duct Provided with transverse and inclined ribs as artificial roughness.Renewable Energy. 2009; 34:2914–22.
34. Karwa R, Chitoshiya G. Performance study of solar air heater having v-down discrete ribs on absorber plate. Energy. 2013; 55:939–55.